THE JOURNAL OF PHYSICAL CHEMISTRY Letters

Letter

pubs.acs.org/JPCL

Intrinsic Edge Asymmetry in Narrow Zigzag Hexagonal Heteroatomic Nanoribbons Causes their Subtle Uniform Curvature

Pavel V. Avramov,*[,†,‡] Dmitri G. Fedorov,[§] Pavel B. Sorokin,[∥] Seiji Sakai,[†] Shiro Entani,[†] Manabu Ohtomo,[†] Yoshihiro Matsumoto,[†] and Hiroshi Naramoto[†]

[†]Advanced Science Research Center, Japan Atomic Energy Agency, 2-4 Shirakata Shirane, Tokai-mura, Naka-gun, Ibaraki-ken 319-1195, Japan

[‡]L.V. Kirensky Institute of Physics SB RAS, Krasnoyarsk 660036, Russia

[§]Nanosystem Research Institute, National Institute of Advanced Industrial Science and Technology (AIST), Tsukuba, 305-8568 Japan

[∥]Technological Institute for Superhard and Novel Carbon Materials, 7a Centralnaya Street, Troitsk, Moscow region, 142190, Russia

ABSTRACT: The atomic and electronic structure of narrow zigzag nanoribbons with finite length, consisting of graphene terminated by fluorine on one side, hexagonal (*h*) *h*-BN, and *h*-SiC were studied with density functional theory. It is found that the asymmetry of nanoribbon edges causes a uniform curvature of the ribbons due to structural stress in the aromatic ring plane. Narrow graphene nanoribbons terminated with fluorine on one side demonstrate a considerable out-of-plane bend, suggesting that the nanoribbon is a fraction of a conical surface. It is shown that the intrinsic curvature of the narrow nanoribbons destroys the periodicity and results in a systematic cancellation of the dipole moment. The in- and out-of-plane curvature of thin arcs allows their closure in nanorings or cone fragments of giant diameter. Using the fragment molecular orbital method, we optimized the structure of a planar giant arc and a closed ring of *h*-BN with a diameter of 105 nm.

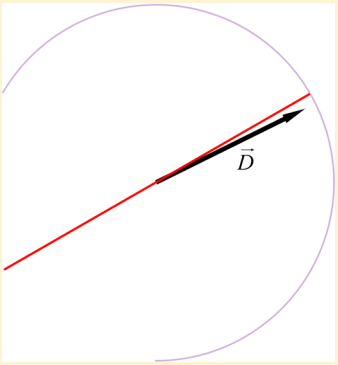

SECTION: Molecular Structure, Quantum Chemistry, and General Theory

The hexagonal atomic lattices of single graphene,[1] hexagonal BN,[2] and SiC[3] layers with one type of interatomic bond consist of two nonequivalent sublattices with one carbon, boron, nitrogen, or silicon atom in a subunit cell. Three major types of nanoribbons can be cut out from the hexagonal (*h*) lattices:[4] armchair (ANR), zigzag (ZNR) and chiral.[5,6] The graphene, *h*-BN, and *h*-SiC ANRs with hydrogen-saturated dangling bonds on the edges have a singlet closed-shell ground state, but the open-shell electronic structure of ZNRs is metastable,[5,7,8] and high spin states can compete with the spin-polarized singlet state. It is shown in Figure 1 that the two kinds of edges in BN are made of the same (zigzag) and different (armchair) types of atoms.

Previously,[9,10] using the elastic plate theory, it has been shown that the edge stress caused by local atomic structure distortions introduce edge-localized intrinsic ripples in free-standing graphene sheets with unsaturated edge dangling bonds. A compressive stress along the zigzag and armchair edges results in an out-of-plane warping and several degenerate mode shapes. The edge stress also leads to twisting and scrolling of nanoribbons as seen in the experiments. Spontaneous twist and intrinsic instabilities of pristine graphene nanoribbons have also been studied in atomic simulations.[10] The graphene and BN nanoribbons have received very considerable attention recently.[11−23]

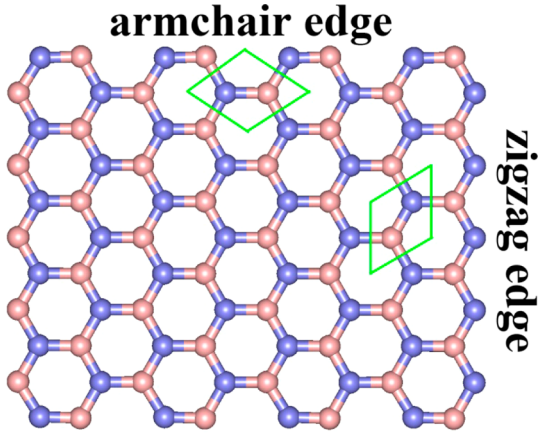

Figure 1. Atomic structure of a fragment of the *h*-BN lattice. A unit cell is made of one B−N group (two equivalent cells are shown in boxes). The armchair edges consist of atoms of both types (B and N), whereas the zigzag edges are made of either B or N atoms.

The stress[24,17,25] and energetic stability[26] of zigzag edges of BN, SiC, and MoS_2 hexagonal planar lattices have been studied

Received: May 17, 2012
Accepted: July 11, 2012
Published: July 11, 2012

Table 1. Properties of Nanoribbons: The Number of Aromatic Rings in Terms of Width *m* and Length *n*, Spin *S*, Effective Radii R_{eff} (Å) of Arcs, HOMO−LUMO Gaps (eV), and Zero Point Corrections (ZPE) in kcal/mol

(*m*,*n*)	system	*S*	DFT functional	basis set	R_{eff}, Å	HOMO−LUMO gap, for α/β spin, eV	ZPE,[a] kcal/mol
				h-BN			
(1,17)	$B_{35}N_{35}H_{38}$	0	HSE	6-21G*	247.4	6.056	
		1	HSE	6-21G*	544.2	0.596/0.497	
		2	HSE	6-21G*	429.7	0.600/0.508	
(1,35)	$B_{71}N_{71}H_{74}$	0	HSE	6-21G*	322.8	6.047	1065.4
		1	HSE	6-21G*	311.1	2.208/1.906	
		0	HSE	6-31G	351.7	6.095	
		0	HSE	6-31G*	334.1	6.154	
		0	HSE	6-311G*	367.2	6.142	1078.7
		0	HSE	cc-PVDZ	375.5	6.062	
		0	B3LYP	6-21G*	365.4	6.340	
		0	B3LYP	6-311G*	422.9	6.446	
(1,62)	$B_{125}N_{125}H_{128}$	0	HSE	6-21G*	275.9	6.053	
		0	HSE	6-31G	281.5	6.101	
		0	HSE	6-31*G	270.3	6.159	
		0	HSE	6-311G*	292.5	6.150	
		0	B3LYP	6-31G	525.8	6.401	1863.2
(3,36)	$B_{146}N_{146}H_{80}$	0	HSE	6-21G*	785.3	5.758	1730.2
		0	HSE	6-311G*	828.9	5.846	1752.0
				h-SiC			
(1,17)	$Si_{35}C_{35}H_{38}$	0	HSE	6-21G*	175.8	1.365	
		1	HSE	6-21G*	323.5	0.226/0.205	
(1,35)	$Si_{71}C_{71}H_{74}$	0	HSE	6-21G*	155.8	1.344	
		1	HSE	6-21G*	189.7	0.183/0.162	
		0	HSE	6-31G*	155.0	1.415	
(1,60)	$Si_{121}C_{121}H_{80}$	0	HSE	6-21G	158.7	0.860	1415.7
		0	HSE	6-21G*	152.3	1.336	1456.8
		0	B3LYP	6-21G	169.6	1.198	1409.6
(3,23)	$Si_{92}C_{92}H_{52}$	0	HSE	6-21G	2518.5	0.021	828.0
		0	HSE	6-21G*	2846.3	0.030	
(3,38)	$Si_{152}C_{152}H_{82}$	0	HSE	6-21G	1916.7	0.017	1345.0
(5,15)	$Si_{93}C_{93}H_{42}$	0	HSE	6-21G*	1657.2	0.005	
(5,23)	$Si_{141}C_{141}H_{58}$	0	HSE	6-21G*	2349.8	0.003	
				One-Side FTG			
(1,35)	$C_{142}H_{37}F_{37}$	0	HSE	6-31G*	363.5	0.160	939.4
		1	HSE	6-31G*	183.3	0.836/0.812	
		0	HSE	6-311G*	237.3	0.152	942.9

[a]Hessians were computed for some representative structures, all of which were found to be true minima.

using density functional theory (DFT) and model potentials. Most of these simulations have been performed for bare monatomic (B, N, Si, and C atoms) edges of BN and SiC triangles or triangular holes in the corresponding lattices. Dangling bonds at a zigzag edge affect the nature of the chemical bonding in the edge hexagonal rings and cause their visible distortion. It was found that the zigzag edges of *h*-SiC and *h*-BN 2D monolayers display visible edge rippling patterns.[17] Termination of the dangling bonds by hydrogen atoms significantly reduces the edge stress.[25]

The electronic structure calculations of the nanoribbons have been reported using the periodic boundary approach (PBC)[5,7,8] and DFT. The structural nonequivalence of both edges of *h*-BN and *h*-SiC ZNRs causes a structural tension and a consequent bending of the nanoribbons and a loss of the periodicity. Because of that, the commonly used PBC model is not suitable for a realistic description of the atomic and electronic structure of *h*-BN and *h*-SiC ZNRs. For graphene ZNRs, the structural nonequivalence of the edges can be introduced by saturation of the edge dangling bonds by different types of atoms (hydrogen atoms from one side and fluorine ones from the other). For narrow ZNRs with heteroatomic hexagonal lattices of *h*-BN, *h*-SiC and one-side fluorine-terminated graphene (FTG) the edge stretching forces do not compensate each other. The narrower the width, the more the plane stretching, because the Young modulus of a nanoribbon is much greater for the bending than for the stretching. Finally, there is a possibility of a subtle bend in the out-of-plane bending resulting in a conical ribbon.

The main goal of this Letter is to study the structure and electronic properties of narrow *h*-BN, *h*-SiC, and FTG ZNRs by means of DFT in the cluster model. Electronic structure calculations of zigzag narrow nanoribbons of different widths (1, 3, and 5 aromatic rings) and lengths (up to 156 Å, Table 1) were carried out using Gaussian.[27] The optimized geometries of each ribbon were obtained using the 6-21G*, 6-31G*, and in some cases other Gaussian basis sets and two different functionals, B3LYP and the long-corrected screened exchange hybrid density functional, HSE.[28,29] The latter functional has been tested in a wide set of materials and shown to accurately reproduce experimental band gaps.[30,31] Furthermore, HSE has

dx.doi.org/10.1021/jz300625t | J. Phys. Chem. Lett. 2012, 3, 2003−2008

also been demonstrated to deliver accurate first and second optical excitation energies in metallic and semiconducting SWNTs.[32,33] HSE/PBC with Gaussian-type basis sets has yielded very accurate atomic structure of multilayered graphenes.[23]

The reason for using several basis sets and functionals is to show beyond doubt that the observed effects are real and not caused by a deficiency in the level of calculations. We conducted the Hessian calculations for a number of representative structures and verified that the structures in this work are indeed true minima. For open-shell electronic structure calculations, we used spin-unrestricted DFT, which results in a different highest occupied molecular orbital to lowest unoccupied molecular orbital (HOMO−LUMO) gap for α and β spin.

The atomic structure of partially open and closed *h*-BN zigzag nanorings was optimized at the B3LYP/6-31G level using the fragment molecular orbital (FMO) method[34] implemented[35] in GAMESS.[36] FMO[37] was applied to zeolites[38] and yielded accurate atomic structure of a silicon nanowire.[39] In this work, the nanorings were divided into fragments of three aromatic rings each. The optimization of the *h*-BN nanoring containing 8484 atoms was performed using the generalized distributed data interface[40] on the PC cluster Soroban containing three nodes equipped with dual hexa-core Xeon CPUs and 2 GB RAM per core, connected by Gigabit Ethernet. In all geometry optimizations, the threshold of 10^{-4} a.u./bohr was used.

The results of electronic structure calculations are presented in Table 1. The larger the total spin of *h*-BN $B_{35}N_{35}H_{38}$ ZNR, the higher the total energy. In $B_{35}N_{35}H_{38}$, the singlet state (S = 0) has the lowest total energy, and the energy of $B_{35}N_{35}H_{38}$ with S = 1 (triplet) is equal to 5.751 eV relative to the singlet; for S = 2, the relative energy is equal to 11.305 eV. A similar (5.378 eV) energy difference for the singlet and triplet states of *h*-BN $B_{71}N_{71}H_{74}$ ZNR is also observed. For *h*-SiC ZNRs ($Si_{35}C_{35}H_{38}$ and $Si_{71}C_{71}H_{74}$), the ground state is a singlet: for both the relative energies of the triplet states are equal to 1.197 eV. On the contrary, at the HSE 6-31G* level of theory, the FTG ZNR $C_{142}H_{37}F_{37}$ is more stable in the triplet state: the relative energy of the singlet state is 0.061 eV.

According to HSE and B3LYP calculations, all narrow *h*-BN, *h*-SiC, and FTG ZNRs in different spin states show a curvature (Figure 2, Table 1). Since the bending effect of ZNRs is subtle, the values of the effective radii depend upon the basis sets and DFT functional. *n* and *m* values, used to mark the clusters, show their width and length (in terms of the number of aromatic rings), respectively. For example, (1,17) $B_{35}N_{35}H_{38}$ means that $B_{35}N_{35}H_{38}$ has the smallest (just one aromatic ring) width and is 17 aromatic rings long.

The singlet states (1,17) $B_{35}N_{35}H_{38}$, (1,35) $B_{71}N_{71}H_{74}$ and (1,62) $B_{125}N_{125}H_{128}$ have the effective radii of 247.4, 322.8, and 275.9 Å, respectively (HSE/6-21G*, see Table 1). The radius of *h*-SiC rings monotonically decreases: it is 175.8, 155.8, and 152.3 Å for 17, 35, and 60 rings, respectively. The curvature tends to converge to some value as the length increases, as verified for large arcs (see below). Visible distortions at both terminal points of each nanoribbon are observed and interpreted in terms of terminal effect. It is necessary to note that the arc of fluorinated graphene is not flat, resembling a conical section bent at the edges (Figure 2).

Increasing the width of ZNRs makes the effective radii larger (i.e., it makes the curvature smaller). For example, (3,36)

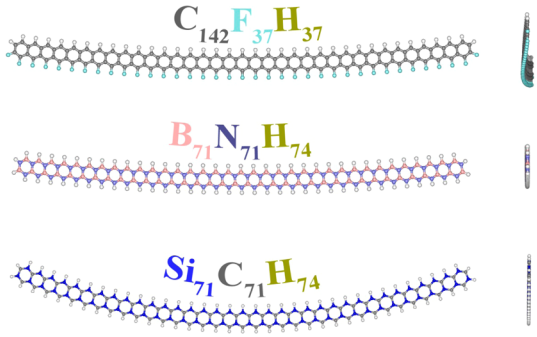

Figure 2. Curved arcs of fluorinated graphene, boron nitride and silicon carbide, along with their side views. All structures are optimized with HSE and 6-31G*. The arc of fluorinated graphene is not flat, resembling a conical section bent at the edges, whereas the other two are nearly planar. Fluorine (light blue), boron (pink), and silicon (blue) atoms face the circle center in each arc.

$B_{146}N_{146}H_{80}$ (S = 0, HSE/6-21G*) has an effective radius (785.3 Å) 2.4 times larger than that for (1,35) $B_{71}N_{71}H_{74}$. Calculations of *h*-SiC (Table 1, Figure 3) reveal a strong

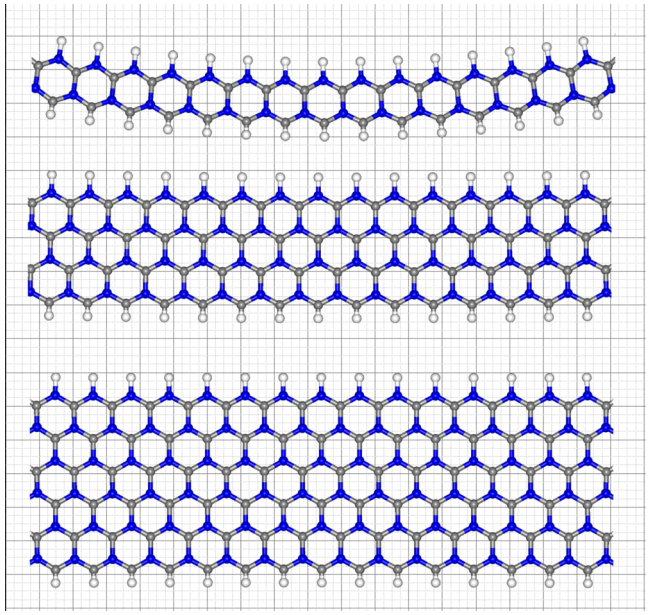

Figure 3. Arcs of silicon carbide with different widths. The arcs of the same length are taken from slightly larger structures optimized with HSE and 6-21G*. Silicon atoms are shown in blue. It is clear that the curvature disappears with increased width; for three layers the curvature is barely seen, and for five layers it is nearly zero.

dependence of the radii upon the width of ZNR: from 200 up to 3000 Å. The strength of the stretching forces is quenched at the width of five rings for *h*-SiC (see Figure 3), and the curvature is barely visible.

It is clear that the curvature destroys the periodicity, and thus the electronic levels of nanoribbons (possibly closed in rings) are quantized rather than continuous. The electronic states of a fully closed ring should resemble the standing waves for a particle in the box.

Increasing the width of *h*-BN and *h*-SiC ZNRs decreases the HOMO−LUMO gap (Table 1). The widest (5,15) $Si_{93}C_{93}H_{42}$ and (5,23) $Si_{141}C_{141}H_{58}$ *h*-SiC ZNRs display almost zero HOMO−LUMO gaps (0.005 and 0.003 eV, respectively)

dx.doi.org/10.1021/jz300625t | J. Phys. Chem. Lett. 2012, 3, 2003−2008

approaching the results of PBC electronic structure calculations of wide *h*-SiC ZNRs.[7] On the other hand, for *h*-BN, the change in the HOMO−LUMO gap with the width is small: the HOMO−LUMO gaps are 6.047 and 5.758 eV for one and three-ring wide ribbons, respectively (HSE/6-21G*).

The band gap of many linear nanosystems follows the quantum confinement effect,[41,42] that is, the band gap decreases with the size, which is explained in terms of the molecular orbital interactions.[41] This effect is also affected by curvature. At the HSE/6-21G* level of theory, the HOMO−LUMO gaps of (1,17), (1,35) and (1,62) *h*-BN arches are 6.056, 6.047, and 6.053 eV, respectively, which does not show a monotonic decrease (this can be related to the maximum in the effective radius for 35 aromatic rings). On the other hand, the HOMO−LUMO gaps of (1,17), (1,35) and (1,60) *h*-SiC are monotonic: 1.365, 1.344, and 1.336 eV, respectively, at the HSE/6-21G* level.

Next, we extend the arcs long enough to accomplish their closure. Using the FMO-B3LYP/6-31G approach, the atomic structure was optimized for the singlet spin state of a set of open ($B_{1751}N_{1751}H_{1754}$) and closed ($B_{2622}N_{2622}H_{2622}$, $B_{2624}N_{2624}H_{2624}$, and $B_{2626}N_{2626}H_{2626}$,) *h*-BN rings with 875, 1311, 1312, and 1313 aromatic rings, respectively. In Figure 4, a typical structure of $B_{2626}N_{2626}H_{2626}$ *h*-BN ring with a detailed structure of a ring fragment is presented. The effective radius of the partially open (approximately 2/3 of the closed rings) $B_{1751}N_{1751}H_{1754}$ ring is equal to 524.9 Å. The atomic structure calculations of the closed rings $B_{2622}N_{2622}H_{2622}$, $B_{2624}N_{2624}H_{2624}$ and $B_{2626}N_{2626}H_{2626}$ revealed that they have typical B−N bond lengths and angles as in other *h*-BN ZNRs, and effective radii of 524.3, 524.8, and 526.2 Å, respectively. This full optimization of the open and closed ZNRs rings shows a good correspondence of the radii of the rings and the arc of *h*-BN ZNR (Table 1): the effective radius of a short (1,62) $B_{125}N_{125}H_{128}$ arc is equal to 525.8 Å.

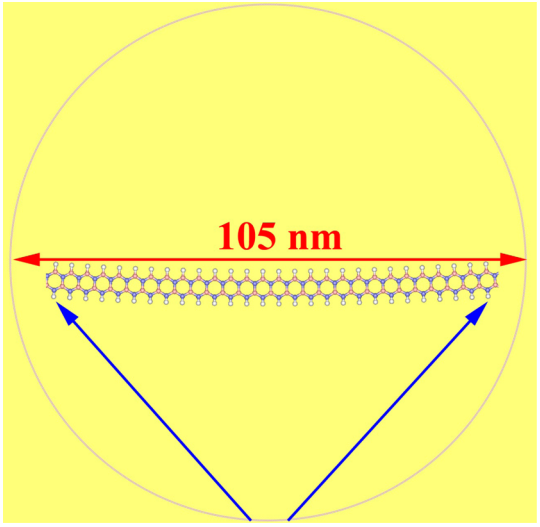

Figure 4. Natural curvature of arcs allows their closure in nanorings. The nanoring of white graphene, boron nitride, is shown. It is fully optimized with FMO-B3LYP/6-31G, and the structure is flat. The chemical formula is $B_{2622}N_{2622}H_{2622}$, and the diameter is 105.0 or 105.6 nm, measured for the inner or outer sets of atoms, respectively. The structure of atoms in the small cut of the nanoring is shown magnified.

A very interesting effect of the curvature is the accumulation of the dipole moment, which we discuss on the example of *h*-BN. A $B_3N_3H_6$ molecule (one ring terminated with hydrogen) has no dipole moment by symmetry. The dipole moment arises when a ribbon is formed, because the asymmetry is introduced in the chain of rings forming an arc because of the zigzag pattern (Figure 1).

In order to understand the calculated dipole moments, we introduce the following conceptual model, which makes it easier to understand the ring-opening effect. The dipole moment $\vec{d}_i$ of an aromatic ring (essentially, $|\vec{d}_i| = d$) is oriented perpendicularly to the arc, and their vector addition yields the total momentum $\vec{D}$ in the conceptual model:

$$\vec{D} = \sum_{i=1}^{n} \vec{d}_i = d \sum_{i=1}^{n} \begin{bmatrix} \cos(\varphi_i) \\ \sin(\varphi_i) \end{bmatrix} \quad (1)$$

where angle φ_i is the polar angle in the plane of the ring. Note that in the actual calculations, the dipole moment in FMO is computed following the two-body expansion of the dipole moments of fragments $\vec{D}^I$ and fragment pairs $\vec{D}^{IJ}$:

$$\vec{D} = \sum_{I=1}^{N} \vec{D}^I + \sum_{I>J}^{N} (\vec{D}^{IJ} - \vec{D}^I - \vec{D}^J) \quad (2)$$

where N is the number of fragments.

It is clear from symmetry consideration that a closed ring (the radial angle $\alpha = 2\pi$) should have a zero dipole moment (see eq 1), whereas the maximum of the dipole moment should be for a half-open ring $\alpha = \pi$, and the dipole moments of large arcs are correspondingly large. This is exactly what we observe in the actual calculations of the nanorings. For the open ring ($\alpha \approx 4\pi/3$, $n = 875$, Figure 5), we got the dipole moment for FMO-B3LYP/6-31G of 442.2 and 218.8 D for the two directions in the plane. On the other hand, a fully closed ring, $\alpha = 2\pi$, $n = 1311$ had almost zero dipole moment (0.1 and 0.3 D for two directions in the plane). The existence of the dipole moment in the nanoribbons determines their electrostatic interaction and the aggregation properties (it can be

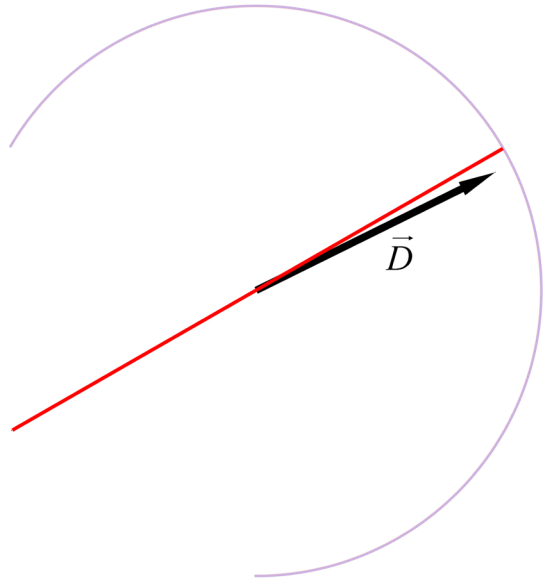

Figure 5. Open BN ring. The red line shows the bisection of the arc dividing it into two equal halves. The calculated total dipole moment (493.4 D) almost coincides with the bisection line. The presence of the ring-opening results in the large dipole moment.

dx.doi.org/10.1021/jz300625t | *J. Phys. Chem. Lett.* 2012, 3, 2003−2008

expected that during a production of nanoribbons many of them are made, which interact with each other). The ring closure completely quenches the dipole moment.

Next, we estimate the bending energy of nanoribbons, by doing HSE/6-21G* calculations of a perfectly linear *h*-BN (1,17) $B_{35}N_{35}H_{38}$ ZNR while fixing the linear structure using symmetry restrictions during optimization. The result is that it takes 0.018 eV to unbend the curved ribbon into a perfectly linear one. Taking into account the length of *h*-BN (1,17) $B_{35}N_{35}H_{38}$ ZNR (4.275 nm), the effect of the curvature for (1,*n*) *h*-BN ZNRs is an energy benefit of 0.004 eV/nm. The HOMO−LUMO gap width of the linear *h*-BN (1,17) $B_{35}N_{35}H_{38}$ ZNR is equal to 6.025 eV, slightly less (by 0.031 eV) than the HOMO−LUMO gap of curved *h*-BN (1,17) $B_{35}N_{35}H_{38}$ ZNR, the latter of which is a true minimum.

The DFT electronic structure calculations of narrow zigzag *h*-BN, *h*-SiC and one-side FTG nanoribbons reveal a subtle universal curvature of the ribbons caused by the structural nonequivalence of the edges. This is a nano effect substantial only for very narrow nanoribbons. Depending on the width and composition of ZNRs, the nanoribbon effective curvature radius varies from 150 up to several thousand angstroms. Narrow nanoribbons of one aromatic ring width have unique electronic properties very different from their sheets, especially for *h*-SiC. The FMO-B3LYP calculations of opened and closed *h*-BN rings allowed us to obtain fully relaxed structures of the open and closed nanorings. By tuning the size and composition of nanoribbons, one can control their band gaps and thus conductance properties, making them an interesting type of material for future applications in nanoelectronics.

AUTHOR INFORMATION

Corresponding Author

*E-mail: avramov.pavel@jaea.go.jp.

Notes

The authors declare no competing financial interest.

ACKNOWLEDGMENTS

This work was supported by JAEA Research fellowship (P.V.A.). P.V.A. also acknowledges JAEA ASRC and the Molecular Spintronics Group for hospitality and fruitful collaboration. D.G.F. thanks Prof. Kazuo Kitaura for many fruitful discussions and the Next Generation SuperComputing Project, Nanoscience Program and Strategic Programs for Innovative Research (MEXT, Japan) for financial support. This work was partially supported by Russian Ministry of Education and Science (Contract No. 16.552.11.7014) (P.B.S.).

REFERENCES

(1) Geim, A. K.; Novoselov, K. S. *Nat. Mater.* **2007**, *6*, 183.

(2) BN - Boron Nitride, *Ioffe Database*, A. F. Ioffe PhTI, Saint Petersburg; URL: http://www.ioffe.ru/SVA/NSM/nk/index.html.

(3) Wu, R. B.; Wu, L. L.; Yang, G. Y.; Pan, Y.; Chen, J. J.; Zhai, R.; Lin, J. *J. Phys. D: Appl. Phys* **2007**, *40*, 3697.

(4) Sirotinin, Yu. I., Shaskolskaya, M. P. *Basics of Crystallography*; Nauka: Moscow, 1979 (in Russian).

(5) Nakada, K.; Fujita, M.; Dresselhaus, G.; Dresselhaus, M. S. *Phys. Rev. B* **1996**, *54*, 17954.

(6) Barone, V.; Hod, O.; Scuseria, G. E. *Nano Lett.* **2006**, *6*, 2748.

(7) Mukherjee, R.; Bhowmick, S. Edge Stabilities of Hexagonal Boron Nitride Nanoribbons: A First-Principles Study. *J. Chem. Theory Comput.* **2011**, *7*, 720.

(8) Sun, L.; Li, Y.; Li, Z.; Li, Q.; Zhou, Z.; Chen, Z.; Yang, J.; Hou, J. G. Electronic Structures of SiC Nanoribbons. *J. Chem. Phys.* **2008**, *129*, 174114.

(9) Shenoy, V. B.; Reddy, C. D.; Ramasubramaniam, A.; Zhang, Y. W. Edge-Stress-Induced Warping of Graphene Sheets and Nanoribbons. *Phys. Rev. Lett.* **2008**, *101*, 245501.

(10) Bets, K. V.; Yakobson, B. I. Spontaneous Twist and Intrinsic Instabilities of Pristine Graphene Nanoribbons. *Nano Res.* **2009**, *2*, 161.

(11) Zhang, Z.; Guo, W. Energy-Gap Modulation of BN Ribbons by Transverse Electric Fields: First-Principles Calculations. *Phys. Rev. B* **2008**, *77*, 075403.

(12) Zheng, F.; Sasaki, K.; Saito, R.; Duan, W.; Gu., B. Edge States of Zigzag Boron Nitride Nanoribbons. *J. Phys. Soc. Jpn.* **2009**, *78*, 074713.

(13) Zheng, F.; Zhang, Y.; Zhang, J.; Xu, K. Effect of the Dangling Bond on the Electronic and Magnetic Properties of BN Nanoribbon. *J. Phys. Chem. Solids* **2011**, *72*, 256.

(14) Chen, W.; Li, Y.; Yu, G.; Zhou, Z.; Chen, Z. Electronic Structure and Reactivity of Boron Nitride Nanoribbons with Stone-Wales Defects. *J. Chem. Theory Comput.* **2009**, *5*, 3088.

(15) Li, J.; Sun, L.; Zhong, J. Strain Effects on Electronic Properties of Boron Nitride Nanoribbons. *Chin. Phys. Lett.* **2010**, *27*, 077101.

(16) Hao, X.; Wu, Y.; Zhan, J.; Yang, J.; Xu, X.; Jiang, M. *J. Phys. Chem. B* **2005**, *109*, 19188.

(17) Jun, S.; Li, X.; Meng, F.; Ciobanu, C. V. Elastic Properties of Edges in BN and SiC Nanoribbons and of Boundaries in C-BN Superlattices. *Phys. Rev. B* **2011**, *83*, 153407.

(18) Salama, I. A.; Quick, N. R.; Kar, A. Laser Synthesis of Carbon-Rich SiC Nanoribbons. *J. Appl. Phys.* **2003**, *93*, 9275.

(19) Zhang, J.; Zheng, F.; Zhang, Y.; Ji, V. First-Principles Study on Electronic Properties of SiC Nanoribbon. *J. Mater. Sci.* **2010**, *45*, 3259.

(20) Lou, P.; Lee, J. Y. Band Structures of Narrow Zigzag Silicon Carbon Nanoribbons. *J. Phys. Chem. C* **2009**, *113*, 12637.

(21) Zhang, H.; Ding, W.; He, K.; Li, M. Synthesis and Characterization of Crystalline Silicon Carbide Nanoribbons. *Nanoscale Res. Lett.* **2010**, *5*, 1264.

(22) Bekaroglu, E.; Topsakal, M.; Cahangirov, S.; Ciraci, S. First-Principles Study of Defects and Adatoms in Silicon Carbide Honeycomb Structures. *Phys. Rev. B* **2010**, *81*, 075433.

(23) Avramov, P. V.; Sakai, S.; Entani, S.; Matsumoto, Y.; Naramoto, H. Ab Initio LC-DFT Study of Graphene, Multilayer Graphenes and Graphite. *Chem. Phys. Lett.* **2011**, *508*, 86.

(24) Deng, J.; Fampiou, I.; Liu, J. Z.; Ramasubramaniam, A.; Medhekar, N. V. Edge Stresses on Non-stoichiometric Edges in Two-Dimensional Crystals. *Appl. Phys. Lett.* **2012**, *100*, 251906.

(25) Liu, Y.; Bhowmick, S.; Yakobson, B. I. BN White Graphene with "Colorful" Edges: The Energies and Morphology. *Nano Lett.* **2011**, *11*, 3113.

(26) Huang, B.; Lee, H.; Gu, B.-L.; Liu, F.; Duan, W. Edge Stability of Boron Nitride Nanoribbons and Its Application in Designing Hybrid BNC Structures. *Nano Res.* **2012**, *5*, 62.

(27) Frisch, M. J.; Trucks, G. W.; Schlegel, H. B.; Scuseria, G. E.; Robb, M. A.; Cheeseman, J. R.; Montgomery, J. A., Jr.; Vreven, T.; Kudin, K. N.; Burant, J. C.et al. *Gaussian 09*; Gaussian, Inc.: Wallingford, CT, 2009.

(28) Heyd, J.; Scuseria, G. E.; Ernzerhof, M. *J. Chem. Phys.* **2003**, *118*, 8207.

(29) Heyd, J.; Scuseria, G. E.; Ernzerhof, M. *J. Chem. Phys.* **2006**, *124*, 219906.

(30) Heyd, J.; Scuseria, G. E. *J. Chem. Phys.* **2004**, *121*, 1187.

(31) Heyd, J.; Peralta, J. E.; Scuseria, G. E. *J. Chem. Phys.* **2005**, *123*, 174101.

(32) Barone, V.; Peralta, J. E.; Wert, M.; Heyd, J.; Scuseria, G. E. *Nano Lett.* **2005**, *5*, 1621.

(33) Barone, V.; Peralta, J. E.; Scuseria, G. E. *Nano Lett.* **2005**, *5*, 1830.

(34) Kitaura, K.; Ikeo, E.; Asada, T.; Nakano, T.; Uebayasi, M. *Chem. Phys. Lett.* **1999**, *313*, 701.

(35) Fedorov, D. G.; Kitaura, K. *J. Chem. Phys.* **2004**, *120*, 6832.

(36) Schmidt, M. W.; Baldridge, K. K.; Boatz, J. A.; Elbert, S. T.; Gordon, M. S.; Jensen, J. H.; Koseki, S.; Matsunaga, N.; Nguyen, K. A.; Su, S.; Windus, T. L.; Dupuis, M.; Montgomery, J. A. *J. Comput. Chem.* **1993**, *14*, 1347.
(37) Fedorov, D. G.; Kitaura, K. *J. Phys. Chem. A* **2007**, *111*, 6904.
(38) Fedorov, D. G.; Jensen, J. H.; Deka, R. C.; Kitaura, K. *J. Phys. Chem. A* **2008**, *112*, 11808.
(39) Fedorov, D. G.; Avramov, P. V.; Jensen, J. H.; Kitaura, K. *Chem. Phys. Lett.* **2009**, *477*, 169.
(40) Fedorov, D. G.; Olson, R. M.; Kitaura, K.; Gordon, M. S.; Koseki, S. *J. Comput. Chem.* **2004**, *25*, 872.
(41) Houg, H.; Koch, S. W. *Quantum Theory of the Optical and Electronic Properties of Semiconductor*; World Scientific: Singapore, 1998.
(42) Avramov, P. V.; Fedorov, D. G.; Sorokin, P. B.; Chernozatonskii, L. A.; Ovchinnikov, S. G. Quantum Dots Embedded into Silicon Nanowires Effectively Partition Electron Confinement. *J. Appl. Phys.* **2008**, *104*, 054305.